Multimode Quasistatic Cavity Resonators for Wireless Power Transfer

Takuya Sasatani, *Student Member, IEEE,* Matthew J. Chabalko, Yoshihiro Kawahara, *Member, IEEE,* and Alanson P. Sample, *Member, IEEE,*

Abstract—The majority of existing wireless power transfer (WPT) solutions are limited to 2-D configurations, which limits mobility when charging electronic devices. What is needed are systems capable of 3-D WPT, which can deliver power everywhere throughout large volumes. Prior work on quasistatic cavity resonance (QSCR) showed promising results for ubiquitous WPT at room scales or larger. However, many challenges remain for QSCR, such as the need for a conductive pole in the middle of the room and the power efficiency that is not high over the entire cavity volume. To address these two issues, this letter introduces a room-scale resonator that possesses a "pole independent" (PI) mode, which can be operated without a pole. It is shown by finite element simulations that by using the PI mode alone, power can be delivered to 93% of the 54 m^3 volume with over 50% efficiency. Moreover, the PI mode and the "pole dependent" (PD) mode, which was used in previous QSCR work can co-exist in the same resonator. These two modes can be selectively stimulated by shifting the operation frequency by less than 1% and no physical switching components are required. It is shown by simulations that power can be delivered with over 66% efficiency to any location in the room by using this dual mode operation.

Index Terms—Multimode, resonator design, wireless power transfer, 3-D charging.

I. INTRODUCTION

RESONANT wireless power transfer (WPT) offers the promise for power delivery over mid-range and at high efficiency [1]–[4]. However, truly ubiquitous WPT, which allows devices to be seamlessly charged as they simply enter a WPT enabled space, still remains a challenge; existing solutions are typically limited to 1-D ("charging cradles") or 2-D configurations ("charging mats") [5], [6]. In recent work, a route towards ubiquitous WPT was proposed using a technique known as quasistatic cavity resonance (QSCR). This technique uses enclosed metallic cavities containing a central conductive pole with discrete capacitors inserted in a gap in the pole, such that one of the resonant modes of the cavity enters sub-wavelength operation. This allows the magnetic fields to permeate the interior of the cavity while confining electric fields to the discrete capacitors. High efficiency (>50%) operation was demonstrated throughout
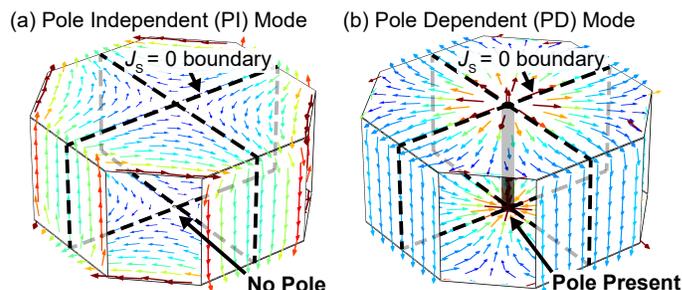
Fig. 1. The surface current of each mode. Color represents magnitude (red, large; blue, small). The $J_s = 0$ boundary indicates the boundary where the normal component of the surface current is 0.

most of the volume of a room sized (4.9 m × 4.9 m × 2.3 m) QSCR [7].

However, there are still several drawbacks to this approach and this letter seeks to address two of them. The first challenge is the need for a conductive pole in the middle of the room, which limits space. The second challenge is the $1/r$ decay of the magnetic field intensity with increasing distance from the pole. Since the magnetic flux crossing the receiver coil decreases near the walls, the WPT efficiency decreases as well [7]. We address these two issues by proposing a room-scale QSCR, which possesses a "pole independent" (PI) mode (Fig. 1a). The PI mode exists whether the pole is present or not. Also, it is shown that the PI mode can co-exist with the "pole dependent" (PD) mode (Fig. 1b), which resembles the mode used in previous QSCR work. The PI mode shows a magnetic field distribution which covers the low WPT efficiency zones of the PD mode and these two modes offer a path to alleviating the two problems mentioned above. Additionally, we will further show that the QSCR technique can be extended to non-fully-enclosed structures, which is not obvious. This extension is necessary since practical room environments require open areas such as doors and windows. Our analysis begins below with a description of the modified QSCR.

II. QSCR TOPOLOGY AND MODE STRUCTURE

The proposed room resonator is shown in Fig. 2a and a unit cell for use in later analysis is shown in Fig. 2b; the unit cell is 1/4 of the whole structure. The proposed resonator differs from the QSCR in [7] in two ways: the conductive portions of the walls and ceiling/floor in the corners of the structure are removed and capacitors are installed at each edge where the walls and ceiling/floor meet. The wall width is denoted as $w \cdot p$, where p is the fraction of the total width (here, $w = 4.9$ m), and p is a variable. The capacitors on the edges were all set to the same value C_2 with a uniform distribution across the

edge. The pole consists of copper[1] with high conductivity since limiting losses here is critical in the small cross section of the pole. It is noted that this pole refers to an electrically conductive pole. The walls consist of aluminum[2], which is comparatively inexpensive and low density, both desirable properties for ease of construction of large cavities. Using this structure, the simulated results for the surface currents and the magnetic field of each mode are shown in Fig. 1 and Fig. 3, respectively. The PD mode resembles the mode used in previous QSCR work, with a magnetic field circulating the pole, and strongest near the pole. Conversely, the PI mode induces no current in the pole and the current flows *only* through the walls and ceiling/floor, subsequently generating a stronger magnetic field near the walls. Taken together, the magnetic field is strong throughout a much larger volume of the cavity than for either mode alone, thus offering the potential for higher efficiencies throughout the space when using dual mode operation.

III. Tuning and Control of The Resonant Modes

We next proceed with analysis to determine the resonant frequency of each mode, ω_0. To do this, we treat the structure as having an equivalent inductance, L, and capacitance C, such that the resonant frequency is given by the expression for a LC tank: $\omega_0 = 1/\sqrt{LC}$. C is set by use of discrete capacitors. This leaves only the inductance left to compute; however, analytic expressions are not easily derived. We instead used a finite element method (FEM)-based approach for computing the inductance of a structure with fixed geometry.

First note that, for both modes, the surface current, J_s, never crosses the $J_s = 0$ boundaries shown in Fig. 1a and Fig. 1b. The current flows through the *wall-ceiling-pole-floor-wall* loop in the PD mode and the *wall-ceiling-wall-floor-wall* loop in the PI mode, which both loops are closed in a single unit structure as shown in Fig. 2b. Therefore, the total current can be treated as a combination of 4 independent current loops, which are coupled to each other. Thus, the magnetic energy of *one* unit current loop, w_m, is a quarter of the total energy in the full volume due to the symmetry of the structure. If a FEM simulation is first done using a known capacitance value and eigenmodes are solved for, then the software can subsequently be used to evaluate the structure's total magnetic energy, α, and the current of *one* unit loop I. Dividing α by 4 yields the magnetic energy that a single unit cell possesses: w_m. Finally, the inductance can be retrieved by noting that the energy stored in an inductor (one unit cell here) is $\alpha/4 = w_m = 1/2LI^2$, and w_m and I both are known from simulation leaving only L to be solved for. Once L is computed, the discrete capacitance C can be chosen to yield a desired resonant frequency:

$$\omega_0 = \frac{1}{\sqrt{C \cdot \frac{2w_m}{I^2}}} = \frac{1}{\sqrt{C \cdot \frac{\alpha}{2I^2}}} \qquad (1)$$

Considering the capacitor positions shown in Fig. 2a and the current paths shown in Fig. 2b, the capacitance inserted in the unit current loop of the PD and PI mode can be calculated as

---

[1] Conductivity of 5.8×10^7 S/m, referring to IACS copper standard.
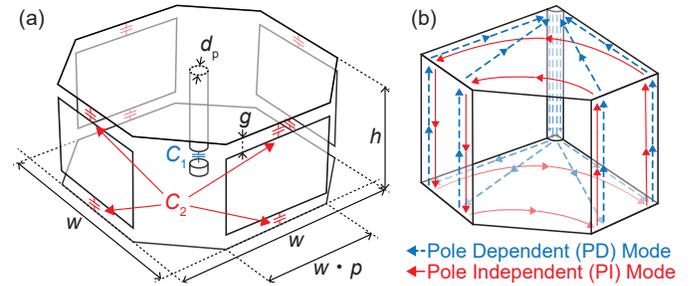[2] Conductivity of 3.445×10^7 S/m, referring to 1100 aluminum alloy.

Fig. 2. The geometry of the proposed resonator. p is the proportion of the width of the wall. The height h, the width w, the diameter of the pole d_p, and the gap for the capacitors g were set to 2.3 m, 4.9 m, 0.072 m, and 0.025 m, respectively. (a) Full structure. (b) One unit structure which consists of a quarter of the full structure. The arrows represent the current path for each mode and the gap for the capacitors are neglected for simplicity.
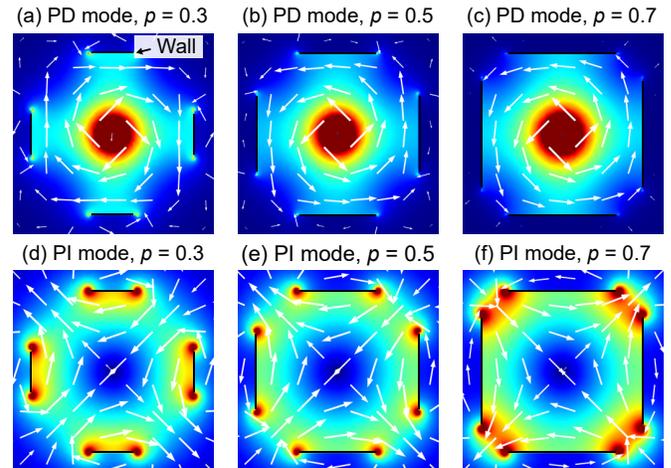

Fig. 3. Magnetic field intensity on plane $z = 0$ for each mode and wall width proportion p. The coordinates refer to Fig. 5. Color represents magnitude (red, large; blue, small).

$C_{\text{PD}} = C_1 C_2/(2C_1 + 4C_2)$ and $C_{\text{PI}} = C_2/8$, respectively, by applying basic circuit analysis. By using this and Eq. (1), the two resonant frequencies can be quickly tuned independently. The resonant frequency of the PD mode f_1 and the PI mode f_2 were set to 1.32 MHz and 1.33 MHz, respectively through the above mentioned process using FEM simulation. In the following, it is assumed that a dynamic impedance tuning circuit is used in the reciever (RX) side to switch between the two resonant frequencies and track the maximum efficiency conditions [2], [8], [9]. It is noted that when the distance in frequency between these two resonances was much smaller than the bandwidth of the room resonator, they could not be excited independently. This bandwidth was narrower than 0.5 kHz throughout this study. Also, we note that in some cases, the resonant frequency from Eq. (1) was different from simulation by approximately 3%, and so some manual tuning using FEM software was necessary. Next, to gauge the effect of having openings in the cavity walls, the wall width proportion p was varied from 0.3 to 0.7 with an interval of 0.1. The figure of merit that was monitored was the simulated Q-factors of each mode, which are presented in Fig. 4a. Importantly, the Q-factor of the PD mode was approximately constant, demonstrating that the QSCR operation can be extended to non-enclosed structures. On the other hand, the Q-factor drops for the PI mode with longer walls; however,
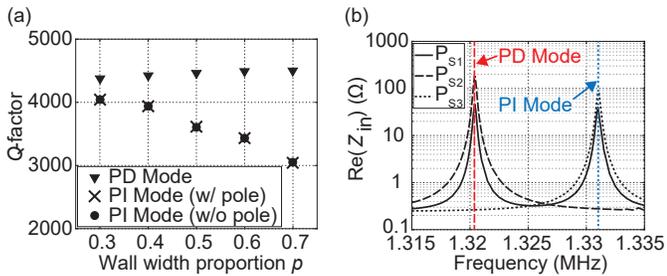
Fig. 4. Evaluation of each mode. (a) The Q-factor of each mode. The capacitor values (C_1, C_2) for $p = 0.3, 0.4, 0.5, 0.6, 0.7$ are $(8.3\text{ pF}, 25.3\text{ pF})$, $(8.2\text{ pF}, 30.4\text{ pF})$, $(8.1\text{ pF}, 36.3\text{ pF})$, $(8.0\text{ pF}, 43.2\text{ pF})$, $(7.9\text{ pF}, 51.7\text{ pF})$, respectively. (b) The input impedance of the source resonators when there are no RX resonators coupled to the room. The peaks represent each mode.

the distribution of the magnetic field intensity of each mode (Fig. 3) also changes with varied p, which subsequently alters the coverage of where WPT efficiency is high. Therefore, it is also necessary to consider the WPT coverage in the selection of p. In both cases, the magnetic fields were approximately uniform in the z-direction.

In order to stimulate these modes as required in a practical WPT system, a source coil resonator was used to couple to the resonant modes of the room resonator. Two configurations were considered for the positions and operations of the source resonators. The first configuration is to couple a single source resonator to *both* modes, by placing the source resonator at positions such as P_{S1} shown in Fig. 5. In this configuration, the two modes can be selectively stimulated by changing the operating frequency by less than 1% or simultaneously stimulated by using a dual-tone input. The second configuration is to use a pair of source resonators solely coupled to each resonant mode. This can be achieved by placing the source resonators at positions such as P_{S2} and P_{S3}, where they are coupled to the PD and PI mode, respectively. In order to confirm that each mode can be stimulated as intended, the input impedance Z_{in} for each source resonator position were evaluated through EM simulations based on FEM. In this case, the wall width proportion p was fixed to 0.5 and there were no RX resonators placed inside. The source resonator is specifically a $300\text{ mm} \times 300\text{ mm}$ square helix resonator composed of copper wire with 4 turns, 10 mm pitch, with resonant frequency tuned to 1.325 MHz using a series capacitor; its Q-factor was 370. The real part of the input impedances are shown in Fig. 4b and it can be seen that the source coil is coupled to each mode as intended at the desired frequency. For the dual coupling case, which the source resonator is positioned at P_{S1}, the input impedance is approximately the same for each mode. This simplifies the design of the power amplifier stage for either finite impedance power source or voltage source-based operation [2]–[4].

IV. POWER TRANSFER EFFICIENCY

Having described the operation of the proposed multimode QSCR, we lastly will determine the WPT efficiency between the QSCR and RX. To do this we use straightforward, albeit approximate, techniques in coupled mode theory (CMT) to extract efficiency throughout the full 3-D volume using FEM simulation to get necessary parameters. Additionally,
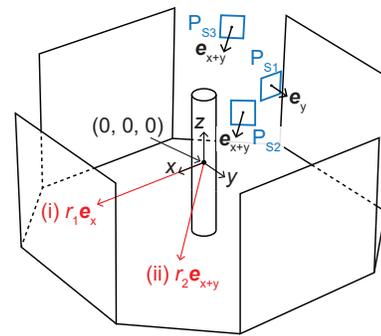

Fig. 5. Configurations in EM simulations. The ceiling and the capacitors are not illustrated for the sake of simplicity. P_{S1}, P_{S2}, and P_{S3} are the positions where the source resonators were placed at and were set to $(-1, 0, 0.8)$ m, $(-0.5, 0.5, 0.8)$ m, and $(-w\frac{p+1}{2}, -w\frac{p+1}{2}, 0.8)$ m, respectively. The vectors on the source resonators shows the normal vectors of the source resonator. $\boldsymbol{e}_x$, $\boldsymbol{e}_y$, and $\boldsymbol{e}_{x+y}$ are unit vectors, whereas $\boldsymbol{e}_{x+y} = (\boldsymbol{e}_x + \boldsymbol{e}_y)/\sqrt{2}$. P_{S2} and P_{S3} are coupled to the PD and PI mode, respectively and P_{S1} is coupled to both modes. Line (i) and (ii) represent the series of positions which the RX resonator was placed at for evaluations based on S-parameters.

to confirm the CMT-based results, simulation of efficiency based on S-parameters were also conducted. The RX resonator was assumed to be a 6 turn, $165\text{ mm} \times 165\text{ mm}$ square helix with a Q-factor of 360 and an inductance of 13.1 μH. The source resonator was assumed to be the same as section. III. Importantly, the load impedance was assumed to be the value that maximizes WPT efficiency in all evaluations [7]–[9].

For the CMT-based evaluation, the center of the RX resonator was placed on 50 mm interval grid points within the volume of the room resonator, which can be represented as $|x|, |y| \leq 2.2$ m, $|z| \leq 1.0$ m (excluding a small region around the pole to accommodate finite size of the RX). Since the scale of the room resonator and the RX resonator was approximately 500 times different, it was assumed that the magnetic flux penetrating the RX resonator was uniform. Also, the orientation of the RX resonator was assumed to be the orientation that maximizes WPT efficiency in each position (i.e. all flux was normal to the coil).

The components necessary to determine the maximum WPT efficiency between two resonators are the coupling rate κ and the Q-factors of the two resonators [7]. The coupling rate was calculated using the total magnetic energy of the QSCR and the magnetic flux penetrating the RX resonator as in the techniques developed in previous work [7], [10]. The obtained maximum, minimum, and average WPT efficiency throughout the volume are shown in Tables. I, II, and III. These tables represent the PD mode, PI mode, and dual mode operation, respectively. The dual mode operation table shows the result when the resonant mode with a higher efficiency at a given RX resonator position is selectively stimulated. The simulated results using the original QSCR topology are also presented in Table. I for reference [7]. It can be seen that when the wall width proportion p is set to 0.7, the WPT efficiency exceeds 66% at any part of the volume by dual mode operation. This result agrees with the magnetic field distribution plots of $p = 0.7$ shown in Fig. 3, where the two modes are a good complement to one another in terms of magnetic field intensity. Moreover, it is discovered that by using the PI mode alone, over 50% efficiency can be obtained in 93% of the volume
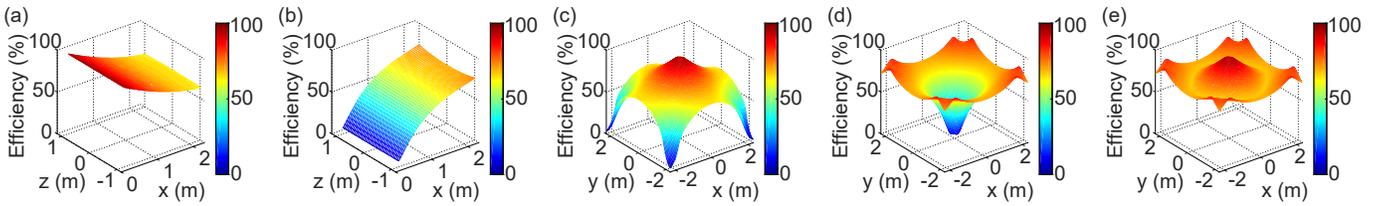
Fig. 6. WPT efficiency at each position. The wall width proportion p is fixed to 0.7 in all plots. (a) and (b) show the plot on the $y = 0$ plane. (c), (d), and (e) show the plots on the $z = 0$ plane. The coordinates refer to Fig. 5. (a) and (c) represent the PD mode. (b) and (d) represent the PI mode. (e) represents the dual mode operation and is a combination of (c) and (d).

TABLE I
WPT EFFICIENCY BY POLE DEPENDENT (PD) MODE

Wall width proportion p	QSCR	0.3	0.4	0.5	0.6	0.7
Maximum efficiency	95%	95%	95%	96%	96%	95%
Minimum efficiency	6%	2%	2%	2%	2%	2%
Average efficiency	63%	60%	61%	62%	62%	63%
Positions over 50 % eff.	84%	75%	78%	81%	83%	84%
Positions over 75 % eff.	20%	19%	19%	20%	20%	20%

TABLE II
WPT EFFICIENCY BY POLE INDEPENDENT (PI, POLE-LESS) MODE

Wall width proportion p	0.3	0.4	0.5	0.6	0.7
Maximum efficiency	88%	87%	87%	87%	87%
Minimum efficiency	12%	11%	10%	9%	7%
Average efficiency	69%	69%	68%	67%	65%
Positions over 50 % eff.	93%	93%	91%	89%	86%
Positions over 75 % eff.	34%	38%	36%	30%	21%

TABLE III
WPT EFFICIENCY BY DUAL MODE OPERATION

Wall width proportion p	0.3	0.4	0.5	0.6	0.7
Maximum efficiency	95%	95%	96%	96%	95%
Minimum efficiency	40%	47%	53%	61%	66%
Average efficiency	75%	76%	76%	76%	75%
Positions over 50 % eff.	100%	100%	100%	100%	100%
Positions over 75 % eff.	53%	56%	55%	49%	41%

with $p = 0.4$; albeit, orientation of the RX remains an issue. Overall this coverage of WPT is superior to the original QSCR structure which requires a center pole.

Lastly, the WPT efficiency at each position with wall width proportion p set to 0.7 is plotted in Fig. 6. Figs. 6a and 6b show the results on the $y = 0$ plane using the PD mode and the PI mode, respectively. It can be seen that the efficiency is approximately uniform in the z-axis direction in both modes. Figs. 6c, 6d, and 6e show the results on the $z = 0$ plane using the PD mode, the PI mode, and dual mode operation, respectively. These plots make it clear that coverage in dual mode operation is greatly improved to either mode alone.

In the S-parameter-based evaluation, the source resonator was placed at P_{S2} and P_{S3} of Fig. 5 for the excitation of the PD mode and the PI mode, respectively. The RX resonator was placed on the series of positions represented by lines (i) and (ii) on Fig. 5, with an orientation that maximizes the penetrating magnetic flux. The results obtained by these evaluations are presented in Figs. 7a and 7b, along with the CMT-based results. From these results, it can be seen that the CMT-based evaluations and the evaluations based on S-parameters correspond well, and this confirms the approximate results obtained based on CMT.

V. CONCLUSIONS

In this paper, we proposed a room-scale resonator with two resonant modes in order to address two challenges of QSCR: the necessity of the center pole and the null-zone of power
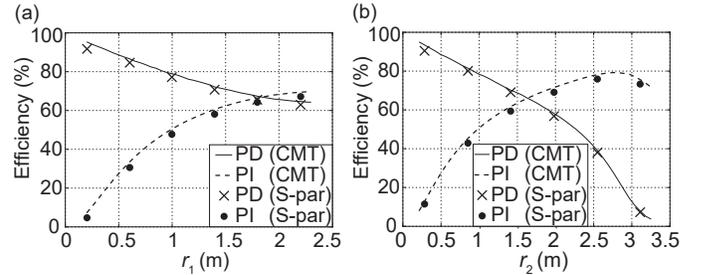

Fig. 7. Comparison of the efficiency obtained by CMT-based evaluations and S-parameter-based evaluations. (a) and (b) shows efficiency on line (i) and (ii) in Fig. 5, respectively. Note that the CMT-based evaluations neglect the loss of the source resonator.

delivery. Also, it is shown that QSCR can be extended to non-enclosed structures. Through FEM-based simulations, it is shown that by using the "pole independent" resonant mode alone, which can be operated without a center pole, power can be delivered to 93% of the volume in a 54 m^3 room with over 50% efficiency; this is superior to the coverage of the original QSCR study, which requires a center pole. Moreover, it was shown that the proposed resonator can deliver power with over 66% efficiency to any location in the volume by using these two modes selectively.

REFERENCES

[1] A. Kurs, A. Karalis, R. Moffatt, J. D. Joannopoulos, P. Fisher, and M. Soljačić, "Wireless power transfer via strongly coupled magnetic resonances," *science*, vol. 317, no. 5834, pp. 83–86, 2007.

[2] J. Park, Y. Tak, Y. Kim, Y. Kim, and S. Nam, "Investigation of adaptive matching methods for near-field wireless power transfer," *IEEE Trans. Antennas Propag.*, vol. 59, no. 5, pp. 1769–1773, 2011.

[3] A. P. Sample, D. T. Meyer, and J. R. Smith, "Analysis, experimental results, and range adaptation of magnetically coupled resonators for wireless power transfer," *IEEE Trans. Ind. Electron.*, vol. 58, no. 2, pp. 544–554, 2011.

[4] Z. N. Low, R. A. Chinga, R. Tseng, and J. Lin, "Design and test of a high-power high-efficiency loosely coupled planar wireless power transfer system," *IEEE Trans. Ind. Electron.*, vol. 56, no. 5, pp. 1801–1812, 2009.

[5] J. Shin *et al.*, "Design and implementation of shaped magnetic-resonance-based wireless power transfer system for roadway-powered moving electric vehicles," *IEEE Trans. Ind. Electron.*, vol. 61, no. 3, pp. 1179–1192, 2014.

[6] N. S. Jeong and F. Carobolante, "Wireless charging of a metal-body device," *IEEE Trans. Microw. Theory and Techn.*, vol. 65, no. 4, pp. 1077–1086, 2017.

[7] M. J. Chabalko, M. Shahmohammadi, and A. P. Sample, "Quasistatic cavity resonance for ubiquitous wireless power transfer," *PloS ONE*, vol. 12, no. 2, p. e0169045, 2017.

[8] M. Zargham and P. G. Gulak, "Maximum achievable efficiency in near-field coupled power-transfer systems," *IEEE Trans. Biomed. Circuits Syst.*, vol. 6, no. 3, pp. 228–245, 2012.

[9] S. Y. R. Hui, W. Zhong, and C. K. Lee, "A critical review of recent progress in mid-range wireless power transfer," *IEEE Trans. Power Electron.*, vol. 29, no. 9, pp. 4500–4511, 2014.

[10] H. A. Haus and W. Huang, "Coupled-mode theory," *Proc. IEEE*, vol. 79, no. 10, pp. 1505–1518, 1991.